# Local Electric Field and Scattering Cross Section of Ag Nanoparticles under Surface Plasmon Resonance by Finite Difference Time Domain Method

**M. Futamata,*,† Y. Maruyama,‡,§ and M. Ishikawa§,||**

*Nanoarchitectonics Research Center and Nanotechnology Materials Program, National Institute of Advanced Industrial Science and Technology (AIST), 1-1-1 Higashi, Tsukuba 305-8562, Japan, Hamamatsu Photonics Co. Ltd., and Single-Molecule Bioanalysis Laboratory, National Institute of Advanced Industrial Science and Technology, Shikoku, Takamatsu 761-0395, Japan*

*Received: November 11, 2002; In Final Form: March 11, 2003*

Local electric field and scattering cross section on Ag nanoparticles were evaluated by the FDTD (finite difference time domain) method with respect to single-molecule sensitivity (SMS) in SERS (surface-enhanced Raman scattering). As a result, (1) vast enhancement of >300-fold (in amplitude enhancement) in the SMS level was obtained at a junction between two connecting Ag particles with various shapes and sizes in addition to an edge of isolated triangular cylinders. Other sites of the connecting particles and of isolated circular and ellipsoidal cylinders gave only modest enhancement of ca. 20−30-fold. (2) The enormously large electric field at the junction rapidly decays with increasing gap sizes <1 nm, irrespective of particle size or shape. In contrast, the LSP (localized surface plasmon) extinction spectra from connecting particles gradually shift toward those from isolated particles with the gap. Thus, in addition to the dipole LSP excitation, nanostructures such as sharp edges, which yield higher order surface modes, are crucial for the vast enhancement. Two-dimensional ordered structures do not yield any additional enhancement concerning SMS−SERS. (3) A red shift of the LSP extinction peak with decreasing height of Ag particles was reproduced only by use of three-dimensional simulation, while broadening and larger extinction at longer wavelength are given by two-dimensional calculation. (4) Blinking of SERS signal observed for dye and DNA base is most probably due to thermal diffusion of adsorbates between the junction with vast enhancement and ordinary sites with modest enhancement, which was supported by the numerical simulation and also experimentally evidenced by suppression of the phenomena at low temperature.

## 1. Introduction

Surface-enhanced Raman scattering (SERS) has been a well-established phenomenon for more than 30 years, in which the Raman signal from adsorbates on metal surfaces is enhanced by a factor of $10^4-10^6$ due to excitation of the surface plasmon polariton (SPP) of roughened metals and/or due to the "first layer" enhancement including charge-transfer resonance between adsorbates and metals.[1,2] Recent progress in SPM (scanning probe microscopy) in observing nanoscale structures, in addition to a highly sensitive CCD (charge-coupled device) detector, enables us to detect extremely weak spectral signals from individual metal particles or even from single molecules. In fact, there are several groups, including us, who reported vast enhancement corresponding to single-molecule sensitivity in SERS.[3−10] As is well-known, plenty of information can be obtained in SERS such as a molecular structure, orientation, or interaction with neighboring species. In contrast, fluorescence spectroscopy, a preceding single-molecule detection method, yields less informative broad spectra yet useful to identify individual molecules.[11] Thus it is valuable to establish a single-molecule detection method (SMD) with SERS to elucidate elementary reaction process at solid/liquid interfaces. The followings are commonly observed results concerning vast enhancement in SERS:[3−10] (1) so-called hot particles appear with prominent enhancement when surface coverage of adsorbates is ca. several tens to 100 per each Ag particle. (2) At lower surface coverage, less than ca. 1 molecule/particle, blinking of the Raman signal, where the intensity suddenly and repeatedly changes with time, is observed for dye and other biomolecules such as hemoglobin on Ag aggregates. The blinking is attributed to a single-molecule phenomenon, since it is not plausible for many molecules to move or change their orientation at the same time. On the other hand, one should note that amorphous carbon obviously shows similar features, in that sharp Raman bands at around 1580 $cm^{-1}$ change their peak frequencies and bandwidth as well as intensity due to photochemical reaction induced by laser illumination.[12] However, at least in our experiments with quite weak laser power of 70 $\mu W/\mu m^2$ at the excitation wavelength of 488 nm, the blinking of the SERS signal from R6G and DNA base adenine is intrinsic in SMD-SERS, since all the observed Raman bands are safely assigned to vibrational modes from original species. Moreover, accumulated spectra for a long duration of measurement, e.g., for 100 s or longer, do not contain any pronounced Raman bands from amorphous carbon.[10] In addition to polarization dependence, Nie and co-workers[3,4] reported that the distinct particle sizes showed different optimum wavelengths, which does not agree with the theoretical evaluation for LSP extinction.[13] Moreover, resonance Rayleigh scattering spectra are not in accordance with the excitation spectra from those of SERS

* To whom correspondence should be addressed: e-mail m.futamata@aist.go.jp.
† Nanoarchitectonics Research Center, AIST Tsukuba.
‡ Hamamatsu Photonics Co. Ltd.
§ Nanotechnology Materials Program, AIST Tsukuba.
|| Single-Molecule Bioanalysis Laboratory, AIST Takamatsu.

10.1021/jp022399e CCC: $25.00 
Published on Web 07/04/2003

for the same Ag particles.[7,8] The spatial distribution of the enhanced field over Ag aggregates or clusters should be experimentally studied to characterize the hot site or hot particles with vast enhancement.[34] Thus, there are substantial uncertainties about the mechanism of the vast enhancement and origin of the blinking. At this stage, it is invaluable to characterize the local electric field on Ag particles regarding the adsorption sites with vast enhancement as well as other sites with modest enhancement.

Theoretical evaluations have been done for the electric field on metal surfaces to solve the enhancement mechanism since the early stage of SERS study.[2,37] They found the metal aggregates give much higher enhancement than isolated particles with respect to LSP resonance. However, these works were mainly devoted to calculate the averaged enhancement for the whole surfaces of each particle with rather simple shape-assuming monolayer adsorbates. This is because, at the early stage of SERS history, the Raman signal from large number of particles, e.g., 100−1000 in a sampled area of $\phi$ ca. 1 $\mu$m, was detected with a conventional microscope system. Accordingly, the enhancement factor was experimentally obtained as a population-averaged value for the whole particles with various size and shapes. In other cases, the local field was calculated for a particular position where adsorbates are presumably located close to metal particles with rotational symmetry, such as a sphere or an ellipsoid.[2,14,15] Thus, the local electric field of metal particles with complicated features in nanoscale has not been elucidated. Recently, the experimental situation has dramatically evolved, since detailed surface morphology of each particle is feasibly observed at an atomic resolution with SPM technology. Then, one can characterize the relation between surface morphology, LSP extinction, and SERS activity for individual metal particles. Furthermore, spatial distribution of the electric field on metal aggregates will be directly observed with by use of scanning near-field Raman spectroscopy.[32,33,16] Actually, SPM probes or optical fiber probes for near-field optical microscopy are sharpened or modified to improve the spatial resolution or to attach the chemical specificity by use of focused ion beam, electron beam lithography, or UPD (underpotential deposition).[18]

Here, we have theoretically evaluated the local electric field on metal nanoparticles with various shapes and sizes. Since the single-molecule sensitivity in SERS was experimentally obtained only for extremely low surface coverage, e.g., a few molecules per each Ag particle or less,[3−10] adsorbed molecules possibly diffuse between various sites with distinct enhancement factors.[9,10] Therefore, we evaluated the local electric field on Ag nanoparticles instead of an averaged field for the entire Ag surfaces to explore the optimum positions for the SMS−SERS with particular shapes and sizes. Vast enhancement was discussed with respect to the LSP excitation. Because the analytical solutions for the Maxwell equations were obtained only for an isolated sphere or ellipsoid with/without substrates, numerical simulation should be utilized to characterize complicated structures, such as an asymmetrical protrusion or edge-containing structure on metal particles. The electric field and scattering cross section for various metal nanostructures were theoretically evaluated on the basis of the finite element method with volume-integral equations.[19,20] The electric field intensity and the scattering cross section at various wavelengths have been studied for Ag nanowire with various types and sizes in cross section. As a result, they obtained SERS enhancement in excess of $10^{12}$ in the vicinity of isolated nonregular particles such as 4:1 right-angled triangles. In addition, spectral response in scattering cross section and enhanced field under the resonance were studied. Unfortunately, their calculation is restricted to the two-dimensional system, possibly due to the large memory size necessary for their method. This is apparently insufficient, since the electronic properties and thus the LSP extinction must be affected by height (length) of the Ag nanowire. In fact, Van Duyne's group reported that the LSP extinction peak prominently shifts to longer wavelength with decreasing height of the Ag triangular tube in nanosphere lithography.[21] However, the two-dimensional calculation cannot yield a sufficiently large shift to longer wavelength even with modification of the aspect ratio of the ellipsoidal or triangular Ag nanowire as reported in this paper. This is critical to discuss the enhancement and the wavelength dependence by electromagnetic effect (LSP mechanism) for the actual Ag nanoparticles. In this paper, we calculated electrical field in near and far fields of the sample by the FDTD (finite difference time domain) method, which can reduce the memory size necessary for the process by a factor of 100 compared to other methods such as a finite element method or boundary element method.[22] Thus, it enables us to use our PC for two-dimensional or even for three-dimensional simulation. Consequently, we found the dramatic LSP peak shift to longer wavelength with decreasing height of the Ag ellipsoid in accordance with the experimental results. Even in more primitive cases, with two-dimensional calculation, one cannot obtain the electric field for polarization inclined (backward or forward) to the plane where the two orthogonal coordinates are located. These results clearly indicate that the three-dimensional calculation is inevitable to explore the optimum nanostructures with respect to single-molecule detection with SERS.

Regarding to this point, Xu et al.[6] reported the wavelength dependence of the electric field for two neighboring metal particles and the modified structures based on multipole expansion and boundary charge methods in a nonretarded scheme. As a result, they obtained an enhancement of $10^{11}$ at the interstitial sites of two touching Ag spheres. Although they calculated the local field in three dimensions, their sample systems are restricted to sphere and droplet with rotational symmetry, or polygonal particles with wide edge angle (145°). To our best knowledge, there are no detailed reports on the electric field calculation for the connecting spheres, triangles, or tetrahedrons in three dimensions with different sizes and shapes at various wavelengths. In addition, we will show the distinct difference of the wavelength dependence in the LSP extinction and local electric field maximum, which is relevant to discuss the experimental results that the resonant Rayleigh spectra from Ag aggregates are not in accordance with SERS activity.[7,8] Also, the local field was calculated for various spacing and two-dimensionally ordered structures to evaluate the LSP coupling of Ag particles.

This paper consists of three parts: (1) After a brief introduction of the FDTD method, its relevance is confirmed by a simple model system, as this is the first case applied to the SERS system. (2) The local field and the LSP extinction (scattering cross section) are described for Ag nanoparticles with various shapes and sizes, including clusters and aggregates. In addition, the decay length of the enhanced field from the surface, the effective length for the LSP coupling, is reported. Comparison between two- and three-dimensional calculations will also be given with respect to the effect of nanostructure height. (3) The origin of the blinking is discussed from the local field calculation and low-temperature observation of the Raman image from R6G (rhodamine 6G).

## 2. Calculation Method

Maxwell equations are solved for spheres or ellipsoids with or without substrate.[2,14,15,23] However, an analytical solution has not been obtained for other complicated structures such as triangular, tetrahedral particles with/without unsymmetrical protrusions or pit, because isolation of variables in the differential equations is substantially difficult. Therefore, a numerical simulation such as an FDTD method is valuable, which transfers the differential equations to difference equations. Thus the numerical solutions can be obtained at given positions and time after the initial electromagnetic field is given. In the FDTD method, the nanostructure is surrounded by virtual boundaries with an appropriate size, and inside this area is separated into small rectangular meshes with a particular size ($\Delta x \times \Delta y$ meshes, see Figure 1; here the two-dimensional expression is given to simplify the explanation). Namely, the metal particles and surroundings are depicted as a collection of these small meshes with a particular size and dielectric properties.[22] In this system, curl in the Maxwell equations is given by the following equations for TM (transverse magnetic) field:[24]

$$E_z^n(i,j) = C_{\mathrm{EZ}}(i,j)E_z^{n-1}(i,j) + C_{\mathrm{EZLX}}(i,j)[H_y^{n-1/2}(i+{}^1/_2,j) - H_y^{n-1/2}(i-{}^1/_2,j)] - C_{\mathrm{EZLY}}(i,j)[H_x^{n-1/2}(i,j+{}^1/_2) - H_y^{n-1/2}(i,j-{}^1/_2)]$$

$$C_{\mathrm{EZ}}(i,j) = \frac{1-\dfrac{\sigma(i,j)\Delta t}{2\epsilon(i,j)}}{1+\dfrac{\sigma(i,j)\Delta t}{2\epsilon(i,j)}}$$

$$C_{\mathrm{EZLX}}(i,j) = \frac{\Delta t/\epsilon(i,j)}{1+\dfrac{\sigma(i,j)\Delta t}{2\epsilon(i,j)}}\frac{1}{\Delta x}$$

$$C_{\mathrm{EZLY}}(i,j) = \frac{\Delta t/\epsilon(i,j)}{1+\dfrac{\sigma(i,j)\Delta t}{2\epsilon(i,j)}}\frac{1}{\Delta y}$$

$$H_x^{n+1/2}(i,j+{}^1/_2) = H_x^{n-1/2}(i,j+{}^1/_2) - C_{\mathrm{HXLY}}(i,j+{}^1/_2)[E_z^n(i,j+1) - E_z^n(i,j)]$$

$$H_y^{n+1/2}(i+{}^1/_2,j) = H_y^{n-1/2}(i+{}^1/_2,j) - C_{\mathrm{HYLX}}(i+{}^1/_2,j)[E_z^n(i+1,j) - E_z^n(i,j)]$$

$$C_{\mathrm{HXLY}}(i,j+{}^1/_2) = \frac{\Delta t}{\mu(i,j+{}^1/_2)}\frac{1}{\Delta y}$$

$$C_{\mathrm{HYLX}}(i+{}^1/_2,j) = \frac{\Delta t}{\mu(i+{}^1/_2,j)}\frac{1}{\Delta x}$$

Here $\sigma(i,j)$, $\epsilon(i,j)$, and $\mu$ are conductivity, dielectric constant, and magnetic permeability, respectively.

According to these equations, the local electromagnetic field $E^{n-1}$ and $H^{n-1/2}$ at orthogonal coordinates $x = x(i)$, $y = y(j)$ and at times $t = t^{n-1}$ and $t^{n-1/2}$ are calculated, and then $H^{n+1/2}$ and $E^n$ as sequential and time-evolutional responses to the incident electromagnetic field. The first-order Mur scheme was used as an absorbing boundary condition in conjunction with a recursive convolution method for metals with prominent dielectric dispersion in wavelength region studied here.[24] In this paper both two-dimensional (2D) and three-dimensional (3D) calculation were performed to show the validity and possibility of the FDTD method in the SERS−SMS system. However, three-dimensional calculation is restricted only to demonstrate the height dependence of the LSP extinction and local electric field for triangular cylinders or for two touching spheres in comparison with the 2D calculation. Detailed results obtained by the FDTD-3D method will be reported in our forthcoming paper. In the FDTD-2D simulation, metal nanostructures are supposed to be a nanowire with infinite height (length) perpendicular to the cross section with various shapes, e.g., circle, triangle, or ellipsoid. Scattering cross section is evaluated by far-field intensity averaged for the entire direction. Local electric field is evaluated with the maximum field intensity on metal surfaces and sufficiently small mesh size, e.g., 0.25 nm × 0.25 or 0.1 nm × 0.1 nm, where variation of the field is rapid at junctions or surfaces of particles, contrary to less dense mesh size for outside the particles with 1 nm × 1 nm, typically. This is quite useful and efficient to obtain the accurate values in a rather short time, especially in three-dimensional evaluations. Actual calculation was performed for metal nanoparticles with various sizes, shapes, and ordered structures on a PC with an Intel Pentium 4 processor and with Windows XP.

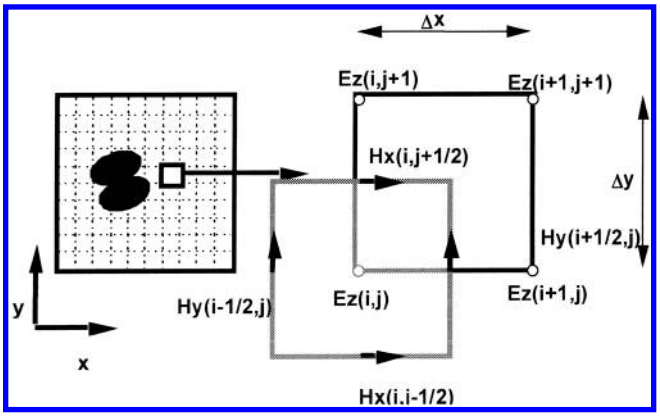


**Figure 1.** Schematic image of a sample system and coordinate used in the FDTD calculation.

## 3. Results and Discussion

**3.1. Relevance of the FDTD Method in the SERS System.** At first, the relevance of the FDTD method was confirmed for the electromagnetic field around the metal particles in the near- and far-field calculations. For this purpose, we adopted an Ag sphere with 10 nm radius placed above the Ag flat substrate with a gap size of 0.5 nm (see Figure 2), as the analytical solution was obtained in the Maxwell equations for this case by use of bispherical coordinates.[14] The plane wave was incident with an angle of 45° and p-polarization (see the inset of Figure 2). Consequently, quite similar local field enhancement of $4.2 \times 10^4$ at 450 nm and $1.29 \times 10^4$ at 400 nm was obtained by the FDTD method at the center between the Ag particle and substrate compared to the values of $4.2 \times 10^4$ at 450 nm and $1.3 \times 10^4$ at 410 nm obtained by analytical solutions[14] as shown in Figure 2. Essentially identical results are obtained for different gap sizes as summarized in Table 1. While these are obtained by the two-dimensional calculation for p-polarization to the substrate, similar results are given by the three-dimensional calculation (see also Table 1) as well as for s-polarization. Thus, we can safely use the FDTD method to evaluate the local electric field in the vicinity of the metal particles. Note that the vast enhancement of $10^{10}$−$10^{11}$ for Raman scattering[31] was predicted

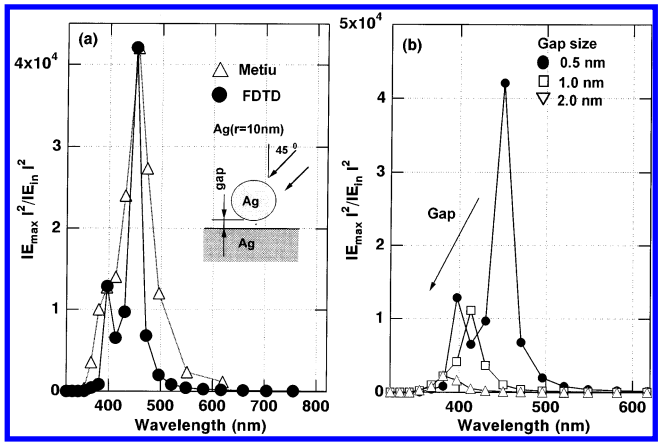


**Figure 2.** Electric field intensity at the gap between the Ag sphere and substrate: (a) results by the analytical solution (△) and FDTD (●) for the Ag sphere with $r = 10$ nm and gap size of 0.5 nm, and (b) results by FDTD for various gap size. Inset: schematic drawing of the sample configuration.

**TABLE 1: Resonance Wavelength and Enhancement Factor for an Ag Sphere ($r = 10$ nm) above Ag Substrate with Different Gap Sizes**[a]

| $d_{gap}$ (nm) | $\lambda_1$[b] (nm) | $I_1$[b] | $\lambda_2$[c] (nm) | $I_2$[c] (FDTD-2D) | $\lambda_3$[c] (nm) | $I_3$[c] (FDTD-3D) |
|---|---|---|---|---|---|---|
| 0.0 | | | 400 | $2.68 \times 10^5$ | | |
| | | | | $2.82 \times 10^5$ | | |
| 0.5 | 450 | $4.2 \times 10^4$ | 450 | $4.20 \times 10^4$ | 450 | $1.53 \times 10^4$ |
| | 410 | $1.3 \times 10^4$ | 400 | $1.29 \times 10^4$ | 370 | $1.16 \times 10^4$ |
| 1.0 | 410 | $7.9 \times 10^3$ | 410 | $1.11 \times 10^4$ | 410 | $7.01 \times 10^3$ |
| 2.0 | 390 | $1.3 \times 10^3$ | 390 | $1.67 \times 10^3$ | 390 | $1.08 \times 10^3$ |

[a] The symbols $I_i$, $I_{max}$, and $I_{in}$ denote the enhancement factor, actual electric field intensity at the gap, and incident field intensity; $I_i = I_{max}/I_{in}$. $d_{gap}$ and $\lambda_i$ are the gap size and resonance wavelength, respectively. [b] Obtained by analytical solutions.[14] [c] Obtained in this work. Essentially identical values $I_1$, $I_2$, and $I_3$ are obtained by the analytical solution and by two- and three-dimensional FDTD calculations, respectively.

for a gap size of 0 nm, which is comparable with those for touching Ag particles with various shapes and sizes as described in the following section. Moreover, this result suggests tremendously large enhancement for Raman scattering from adsorbates at the gap between Ag particles and smooth Ag films, where the propagating SPP is excited with a prism.[16,17,34]

**3.2. Local Field and Scattering Cross Section for the Metal Particles with Respect to SERS Activity.** *3.2.1. Isolated Ag Circular and Ellipsoidal Particles.* Here we do not hold any substrates below the metal particles to evaluate the electric field in the near and far fields for the isolated metal particles. In our real experiments, a glass flat substrate is used to immobilize the metal particles.[9,10] However, a dielectric substrate like a slide glass does not give significant changes in electric field intensity in contrast to the above result for metal substrate, while LSP extinction peaks slightly shift to longer wavelength by a few tens of nanometers. Accordingly, the dielectric substrate was extinguished to reduce size of the sample cell for saving computation time. Scattering cross section for an isolated Ag circular cylinder shows a peak at ca. 370 nm irrespective of size between 10 and 80 nm (Figure 3a). The peak clearly arises from the LSP excitation, of which the wavelength accords with the analytical solutions for spherical particles with the same size.[26] In contrast, two distinct peaks were obtained for triangular structures, at 430 and 500 nm for the right-angle triangle (80 nm × 40 nm) or 400 nm (shoulder) and 450 nm for the symmetrical right-angle triangle (80 nm × 80 nm) (see Figure 3c). The peak for ellipsoid slightly shifts to longer wavelength

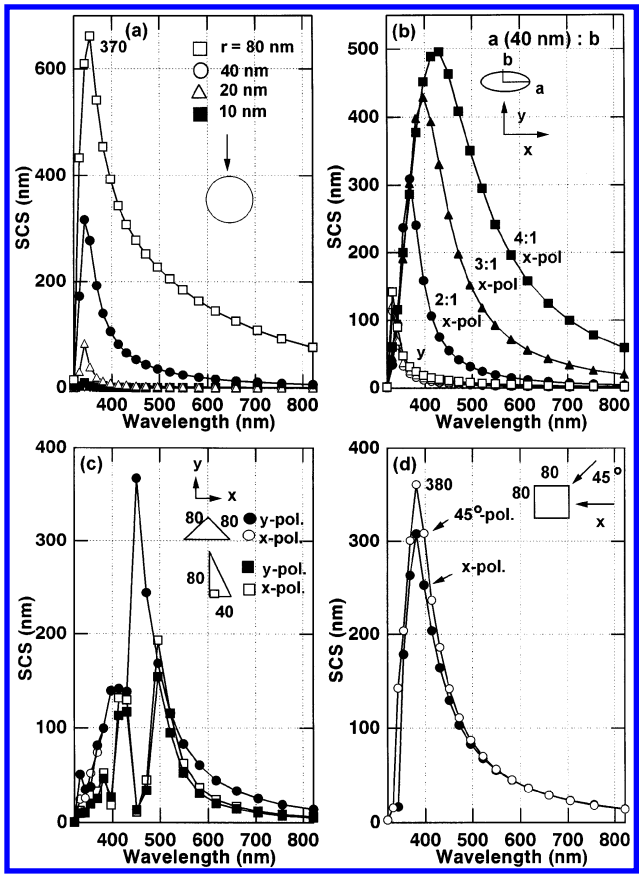


**Figure 3.** Scattering cross section for isolated Ag particles with various shapes and sizes: (a) circular, (b) ellipsoidal, (c) triangular, and (d) tetragonal tubes with different shape, sizes, and polarization. Squares, triangles, and circles in panel b correspond to ellipsoidal particles with aspect ratios of 4:1, 3:1, and 2:1, respectively, for *x*- (solid symbols) and *y*-polarized light (open symbols).

with increasing aspect ratio, e.g., 370 nm (2:1) shifts to 400 nm (3:1) or 430 nm (4:1, see Figure 3b), which is much smaller than the observed values, i.e., 565 nm for the diameter (D) 95 nm and height (H) 48 nm (2:1) ellipsoid to 782 nm for the D 145 nm and H 50 nm (3:1) ellipsoid.[21] For tetrahedral samples with a size of 80 nm (width, W) × 80 nm (H) at the cross section, the LSP peak was obtained at 380 nm irrespective of polarization direction, quite similar to those for circular particles as depicted in Figure 3d. In contrast to the results in two-dimensional simulations, a much larger red shift of the LSP peak was obtained by the three-dimensional calculation. As shown in Figure 4a, the scattering cross section (SCS) peak shifts from 380 nm (for sphere $r_1 = r_2 = 40$ nm) to 450 nm (2:1 spheroid, $r_a = 40$ nm, $r_b = r_c = 20$ nm) and 580 nm (4:1, $r_a = 40$ nm, $r_b = r_c = 10$ nm), which is consistent with the experimental data. In addition, these results fairly accord with analytical solutions for surface mode frequencies determined by geometrical factors.[26] For instance, the resonance condition for an ellipsoidal cylinder is given by $\epsilon'/\epsilon_m \approx -1$ at $\lambda_1 \approx \lambda_2 \approx$ 400 nm, which splits into two branches for a prolate spheroid; $\epsilon'/\epsilon_m \approx -1$ at $\lambda_1 \approx 400$ nm and $\epsilon'/\epsilon_m \ll -1$ at $\lambda_2 \gg 400$ nm [here $\epsilon'$ and $\epsilon_m$ denote the dielectric constants (real part) of particles and media, and $\lambda_1$ and $\lambda_2$ are the first and second resonance wavelength for the surface modes). It suggests that we should utilize three-dimensional simulations to characterize the LSP extinction spectra and local electric field for real metal particles and then to explore the optimum nanostructure. Nevertheless, two-dimensional calculation gives valuable insight into the vast enhancement at the junction as described later.

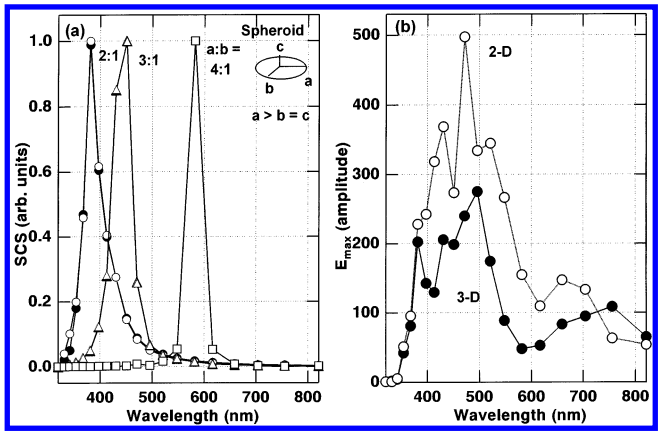


**Figure 4.** Scattering cross section for an isolated ellipsoidal particle with different aspect ratio (a), and the maximum electric field for touching circular particles (b) obtained with FDTD-3D simulation. In panel a, results for *a*- and *b*-polarized light are denoted by open and solid circles, although they are almost identical. Local electric field by FDTD-2D is also shown in panel b (○).

The local electric field on Ag circular cylinder surfaces shows the maximum intensity ($G$) of 10−15 at ca. 380 nm for different sizes, while three peaks were obtained for right-angle triangular cylinder (80 × 40 nm) at 380 nm ($G$ = 180), 430 nm ($G$ = 370), 500 nm ($G$ = 300) with different polarizations (see Figures 5a,c and 6A,B,D). The symmetrical right-angle triangular cylinder shows the maximum ($G$ = ca. 500) at 430 nm with a shoulder at ca. 380 nm (Figures 5c and 6C). With increasing aspect ratio of ellipsoidal particles, where the longer axis is fixed to 40 nm and the shorter axis is changed from 40 to 10 nm, significant spectral changes were not observed (as drawn in Figure 5b). An isolated tetragonal particle [80 nm (W) × 80 nm (H)] shows rather modest enhancement of ca. 110 at 380 nm. Thus, only triangular particles gave vast enhancement at the sharp edge, while only modest enhancement was predicted for isolated circular, ellipsoidal, and tetragonal particles. In addition, wavelength dependence of the scattering cross section is similar to that of the local field maximum for isolated particles. Slight differences of the peak wavelength and width, e.g., for triangular, see Figures 3c and 5c, can be explained on the basis of localization of the LSP field at the edge. The scattering cross section is given by the population-averaged far-field intensity contributed from the entire Ag surface. Accordingly, a particular site like a sharp edge of triangular may not be dominant. In contrast, the electric field maximum is determined by the local structure and the LSP resonance at the particular site, e.g., the enhancement is confined within a few nanometers from the edge, although these are not completely distinguished (see Figure 6C,D). Thus the observed discrepancies between the resonant Rayleigh scattering and the SERS excitation[7,8] were rationalized.

*3.2.2. Local Field Maximum and Scattering Cross Section for Two Touching Ag Particles.* As shown in Figure 7a−c, the scattering cross section for two circular cylinders (radii, $r$ = 40 nm) gives two peaks at ca. 430 and 550 nm in addition to ca. 350 nm, close to 370 nm for isolated particles. These additional peaks unequivocally result from the LSP coupling of the two particles, which gradually shift to longer wavelength with increasing particle size, e.g., to ca. 700 nm for $r$ = 80 nm from ca. 480 nm for $r$ = 10 nm. The pronounced peak was also observed at longer wavelength (520 nm) for ellipsoid (aspect ratio of 1:2, with radii $r_1$ = 40 nm and $r_2$ = 20 nm) in addition to the other peak at shorter wavelength (400 nm, Figure 8). Likewise, the second peak appears for two connecting right-angle triangular particles (80 nm × 40 nm) in an edge-to-edge configuration at >800 and 470 nm, while symmetrical right-angle triangular particles (80 nm × 80 nm) give distinct bands at ca. 400, 470, 580 or 380, 415, 480, and 750 nm according to different configuration as shown in Figure 9a−c. LSP coupling for these particles is efficient for the spacing within about a particle size, e.g., the scattering cross section peak at 430 nm for touching circles ($r$ = 40 nm) approaches and finally merges to the spectra from an isolated particle at 370 nm at a space of 40 nm (Figure 7d), or for touching ellipsoidal particles (see Figure 8d).

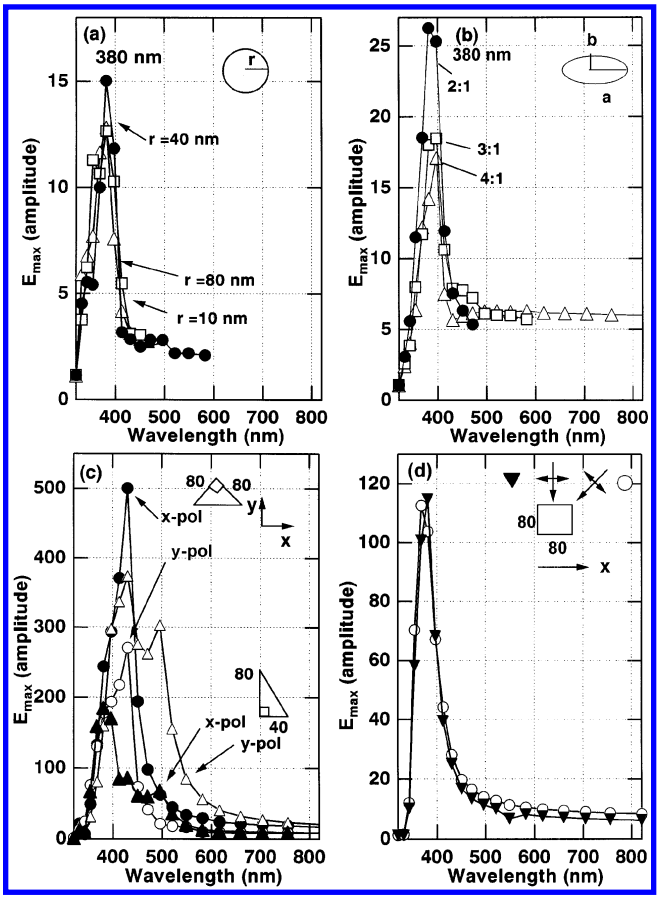


**Figure 5.** Maximum electric field for isolated Ag particles: (a) circular tubes with radii of 10, 40, and 80 nm; (b) ellipsoidal particles with different aspect ratios of 2:1, 3:1, and 4:1 for fixed long axis (40 nm); (c) triangles with different shapes; and (d) tetragonal particles [80 nm (W) × 80 nm (H)] with different polarization. Polarization parallel to the long axis was used for ellipsoidal particles.

Distinct spectral features were obtained for the local electric field maximum compared to the scattering cross section as summarized in Figure 10 and in Figures 7−9. This is again because the local field maximum is determined by the LSP resonance and local nanostructure, whereas SCS is a population-averaged far-field intensity contributed from the entire surface of Ag particles. Several peaks appear at 430, 480, 510, and 700 nm for touching circulars in addition to the original one at 370 nm for the isolated particle. Note that much larger electric field $G$ = 500, which is in a single-molecule sensitivity (SMS) level,[31] is formed at 480 nm for the polarization parallel to the touching direction, in contrast to modest values for isolated circular cylinders. Even for a vertical polarization, a prominent factor of ca. 270 was given at 440 nm. In addition, the maximum peak shifts to longer wavelength with increasing particle size, e.g., from 410 nm for $r$ = 10 nm to 520 nm for $r$ = 80 nm (Figure 11). Quite similar enhancement was obtained at 430 nm ($G$ =

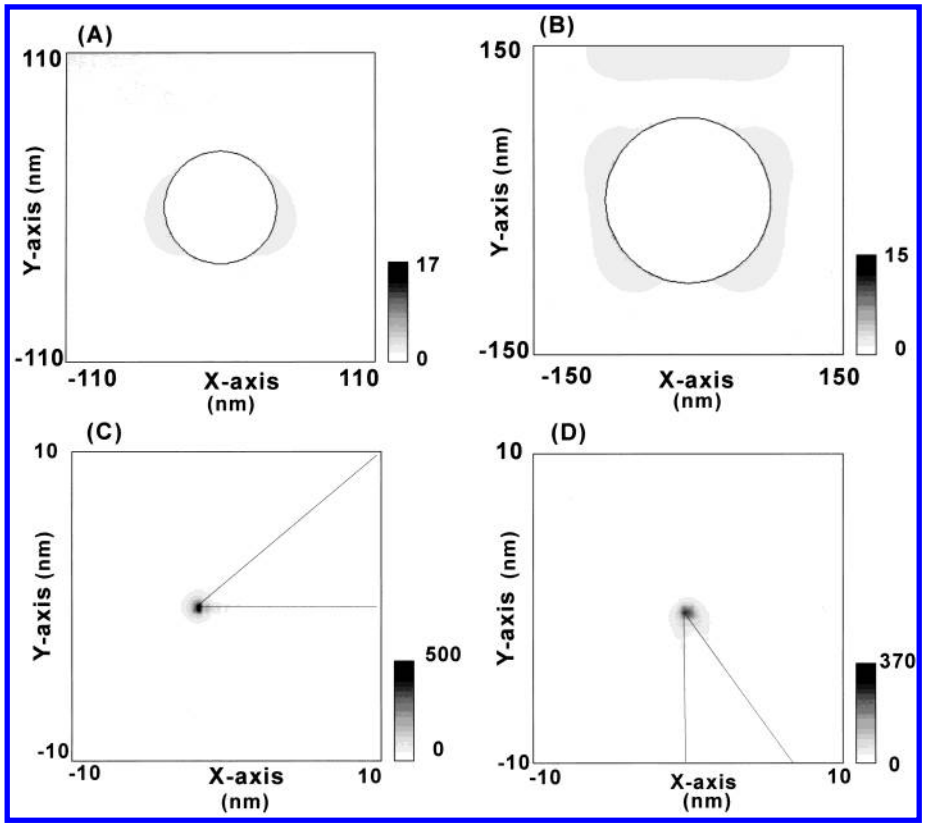


**Figure 6.** Spatial distribution of the electric field on isolated Ag particles at the peak wavelength: (a) circular cylinder ($r = 40$ nm), (b) circular cylinder ($r = 80$ nm), (c) symmetrical right-angle triangular (80 nm × 80 nm), (d) right-angle triangular particles (80 nm × 40 nm). Polarized light along *x*- and *y*-axes was used at 380 nm for panles a and b and at 430 nm for panels c and d, respectively (see also Figure 5). Electric field is shown as an amplitude enhancement relative to the incident field.

600) for touching ellipsoidal particles with the parallel polarization as well as the modest intensity ($G = 60$ at 400 and 520 nm) for vertical polarization (Figure 10b). Rather complicated features at longer wavelength were obtained for triangular particles as the prominent enhancement at the edge is overlapped. The tremendous enhancement factors are obtained for triangular particles with parallel polarization, while slightly modest values similar to isolated particles are predicted for vertical polarization. Right-angle triangular particles (80 nm × 40 nm) give vast enhancement $G = 400$ at 480 nm and $G >$ 800 at >800 nm, while symmetrical right-angle triangular particles give $G > 600$ at 560 nm for side-by-side and 700 nm for edge-to-edge with parallel polarization (see Figure 10c,d).

These features do not essentially depend on the particle sizes, e.g., see Figure 11a for spheres with radii > 20 nm. As depicted in Figures 11b,c and 12, the enhancement rapidly decreases with increasing gap size due to diminished LSP coupling and edge effect, i.e., $G \approx (G_0)/e$ at 1.5 nm gap size and $G = 20$ for 10 nm; here $G_0$ is the enhancement value at the contacting particles. The local field maximum decays in a similar way irrespective of particle sizes between $r = 40$ and 160 nm, as shown in Figure 11b. As proposed, the local field maximum for the triangular edge does not depend on the gap size at the resonance wavelength, i.e., 500 at ca. 400 nm for the symmetrical right-angle particle. However, the enhancement arising from the LSP coupling at the junction with the resonance wavelength of 660 nm rapidly decreases even for triangles at the gap size < 1 nm, similar to the circular particles (Figure 11c). The sharp decay of the local field maximum is clearly explained by the peak shift of the LSP resonance to shorter wavelength and by the decreased coupling with increasing the spacing as shown in Figure 10a (see also Figures 7d and 8d).

In addition, these results indicate that the critical condition to give the vast enhancement at SMS level is the LSP resonance and also the nanostructures such as edges or junctions, where the dense electric field is confined. This is rationalized by the following simulation that only modest electric field was obtained for two tetrahedral particles placed in a side-by-side configuration with sufficiently small spacing of $d < 0.5$ nm. In fact, the maximum enhancement (70 at 380 nm for a gap $d = 0$ nm) is quite similar to that for isolated tetragonal particles (110 at 380 nm, see Figures 11d and 5d). In addition, the scattering cross section for this configuration is similar to the isolated one, as no additional bands are observed at longer wavelength. In contrast, the edge-to-edge configuration of the same tetragonal particles gave the vast enhancement at ca. 550 nm with a shoulder at 400 nm (Figure 11d) as well as an additional peak in scattering cross section at ca. 540 nm (not shown). Conclusively, a sharp edge as well as the LSP coupling is indispensable to give the enormously large enhancement. Note that the junction between touching circular nanowire consists of moderate curvature at the metal and much sharper one at an air-side, which contributes electric field confinement enhanced by the LSP resonance. In addition, we noted that the local field maximum at a small protrusion with sufficiently sharp edge placed on a circular cylinder is quite similar to those for a triangular edge or the junctions of particles, while the LSP spectra are similar to an isolated circular tube. This result suggests two plausible reasons for the discrepancies between the observed wavelength dependence of the optimum size and theoretical predictions:[3] (1) the second particle is located behind the first one, or (2) there is an isolated particle with small protrusions, which could not be imaged due to insufficient spatial resolution of the atomic force microscope (AFM). Thus, the spatial distribution of the

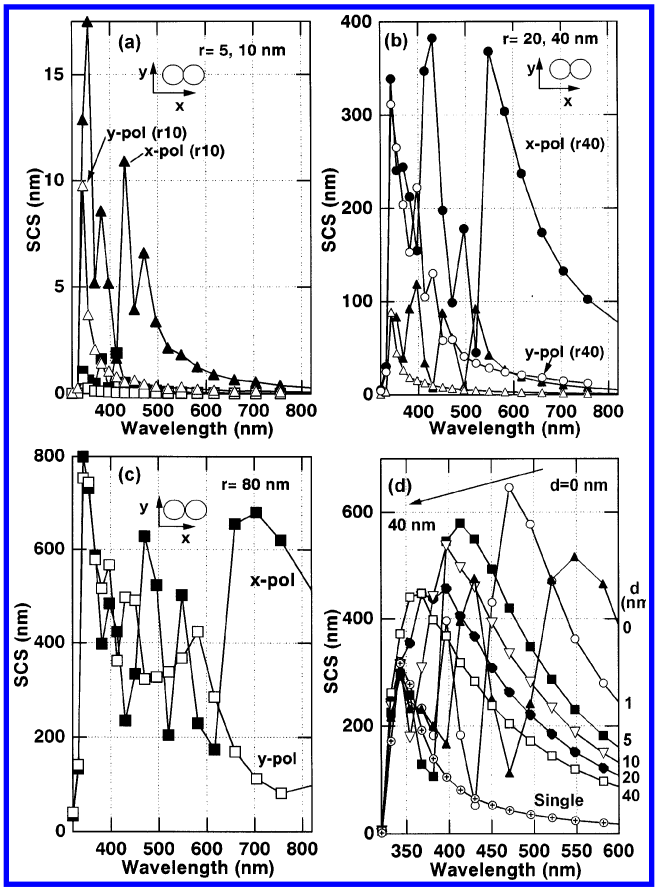


**Figure 7.** Scattering cross section for two touching Ag circular tubes: (a) $r = r_1 = r_2 = 5$ nm (squared) or 10 nm (triangles); (b) $r_1 = 20$ nm (triangles) or 40 nm (circles); (c) $r = 80$ nm for different polarization, and (d) gap size dependence. In Figures 7−13, the symbols of *x* (solid symbols) or *y* (open symbols) denote polarization parallel and perpendicular to the touching axis, respectively. In this figure, solid and open symbols denote the results for *x*- and *y*-polarized light, respectively.

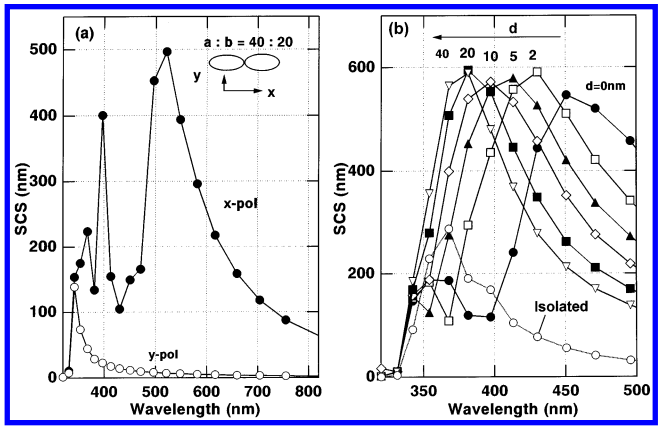


**Figure 8.** Scattering cross sections for two Ag ellipsoids: (a) touching ($r_1 = 40$ nm and $r_2 = 20$ nm); (b) gap size dependence (expanded) for *x*-polarized light.

LSP resonance and local electric field should be further studied by the Scanning Near-field Optical Microscope (SNOM) method in addition to topographic imaging of the metal particles.

Moreover, as shown in Figure 4b, we have confirmed by three-dimensional calculation that the similar enhancement of ca. 300 at 500 nm corresponding to single-molecule sensitivity level in SERS was obtained at the junction and wavelength dependence in the local electric field for two touching Ag spheres. Slightly smaller values compared to the 2D calculation are due to rather large mesh sizes of 0.5 nm × 0.5 nm × 0.5 nm adopted to save computing time, similar to the SCS spectra by different mesh sizes in FDTD-2D. It indicates that the vast enhancement at the junction is already obtained by the two-dimensional nanostructures, although distinct spectra for scattering cross section and the local field maximum were obtained for circular or ellipsoidal cylinder (2D) in comparison with spheres or spheroidal particles (3D; e.g., see Figure 4).

*3.2.3. Multiparticle Systems.* Recently, nanostructures have attracted attention for various purposes, e.g., to elucidate and control a quantum effect in nanowires or quantum dots or to innovate single-molecule devices or molecular processors.[27] Here we studied whether one- or two-dimensionally ordered Ag nanostructures yield additional enhancement in the local electric field due to a possible cooperative coupling of the LSP resonance. Conclusively, the enhancement factor observed at ca. 470 nm was not significantly changed with increasing the number of particles (see Figure 13c,d). This is because the maximum intensity is primarily determined by the local structure at each junction, and also because the vast enhanced field between the neighboring particles sharply decays within 1 nm. Thus the third particle cannot directly interact with the first particle for additional enhancement, because of too long separation between them. In fact, the enhanced field obtained for three and four connecting Ag particles in a line shows quite similar wavelength dependence to two touching particles. In contrast, the SCS peak possesses slightly distinct features that the longer wavelength component becomes dominant with increasing the particle numbers as shown in Figure 13a,b (see also Figure 7b). Very crudely, this is similar to the results for extended aspect ratio of ellipsoidal particles and compatible with rather long decay length of the coupling. We note that a new LSP peak does not appear, while the LSP peak at longer wavelength increases its intensity with increasing particle number. Accordingly, two-dimensional ordering of metal nanowire does not provide any additional enhancement in the local electric field maximum with respect to SMS−SERS. Thus the metal aggregates are not always necessary, but two touching particles are sufficient to give SMS−SERS. In actual experiments, however, the aggregated particles are useful to find hot particles, as the vast enhancement is obtained for polarization parallel to the connecting direction. Yet, we should also note these results are obtained by the two-dimensional calculation, while distinct properties in scattering cross section and local electric field are proposed in the three-dimensional calculation. Preliminary but similar results were obtained by three-dimensional FDTD simulation with rather large mesh sizes of $\Delta x = \Delta y = \Delta z = 1$ nm. The largest peak was obtained at 500 nm with an enhancement factor of ca. 300 in addition to a weaker peak at 400 nm, whereas the third spherical particle does not yield additional SCS peaks nor additional enhancement to two touching spherical particles. Thus, we can safely conclude that third particles aligned at the surroundings of two touching Ag nanostructures do not yield any additional enhancement in the local electric field with respect to SMS−SERS. (Since our target is to explore the optimum nanostructure possessing SMS in SERS, these discussions are concerning the maximum local field. Averaged field intensity for the entire Ag surface may give significantly different properties for isolated Ag particles, e.g., see ref 37, or in one- or two-dimensional ordered structures.)

The noble theory of SERS developed by Otto[28] using dynamic charge transfer (DCT) explicitly accounts for the first-layer effect and blinking of single-molecule SERS for adsorbates with

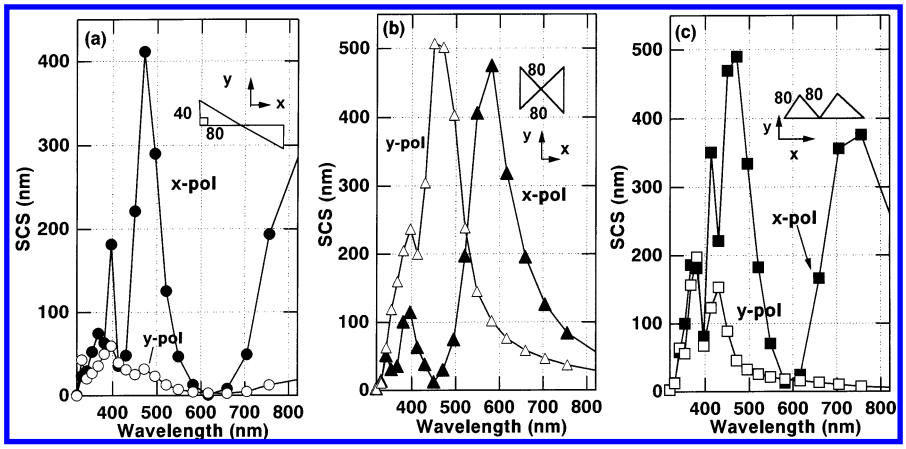


**Figure 9.** Scattering cross section for two touching Ag triangles: (a) edge−edge of right angle ($r_1$ = 80 nm, $r_2$ = 40 nm), (b) edge−edge of equilateral (80 nm × 80 nm), and (c) side−side of symmetrical right-angle particles for different polarization.

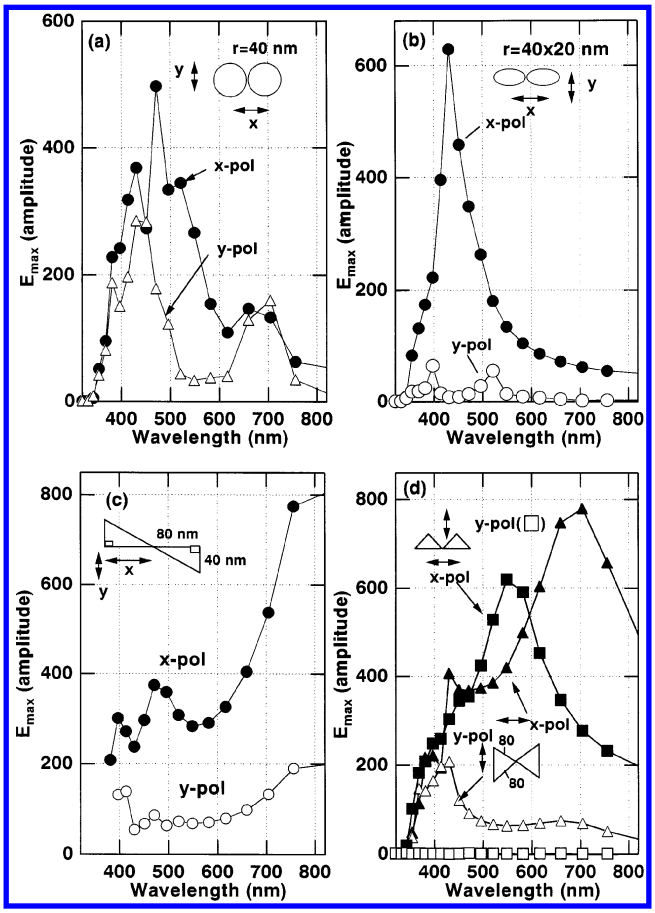


**Figure 10.** Local electric field maximum for two touching Ag particles: (a) circular, (b) ellipsoidal tubes, (c) right-triangular, and (d) symmetrical right-triangular particles with different polarization. In addition, the value for the spacing of 1 nm was also depicted in (a).

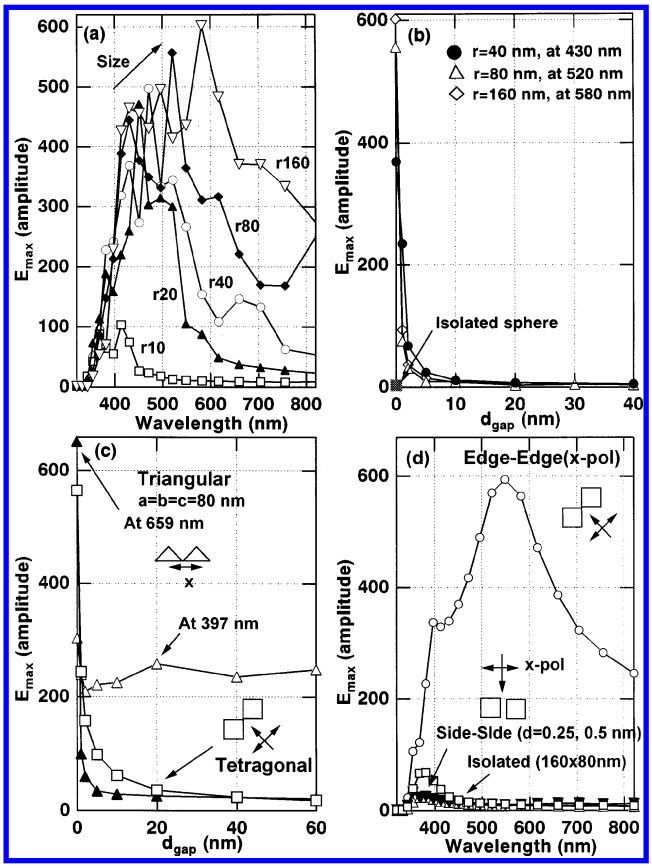


**Figure 11.** Local electric field maximum for two touching Ag circular (a, b) and triangular (c, d) particles: (a) for various circle sizes, (b) spacing dependence for circular tubes with different radii, (c) spacing dependence for triangular and tetragonal, and (d) for tetragonal with different configurations. Spacing dependence was evaluated at the wavelength that gives the maximum electric field intensity at *d* (spacing) = 0 nm (see also Figure 10).

an appropriate lowest unoccupied or highest occupied molecular orbital (LUMO or HOMO) with respect to the Fermi level of metal and excitation wavelength. This is based on electron spilling out at a finite size of boundary such as at roughened surfaces or particles, and thereby interacting with adsorbates. Also it was well confirmed by experimental results on the first layer SERS and Surface Enhanced Infrared Absorption (SEIRA).[1,28] Then, it seems that orientation changes, which yield distinct DCT efficiency and thus enhancement as well as diffusion of molecules, possibly cause the blinking. Unfortunately, for SMS−SERS, we do not have sufficient experimental data for chemical specificity of adsorbed molecules, their HOMO/LUMO features, and location of adsorbed molecules on Ag particles to confirm his theory. Instead, the observed data concerning SMS−SERS can be explained even only with the coupled LSP excitation of each metal particle and the edge effect as it gave sufficiently large enhancement factors. Possible evidence to support this is the fact that the observed SERS spectra from R6G and adenine are nearly identical to those from bulk solution state, indicating no specific interaction with Ag surfaces and/or no electronic resonance via possible charge transfer state formed upon adsorption.[10,25] Nevertheless, additional enhancement, e.g. the first-layer effect for chemisorbed species or

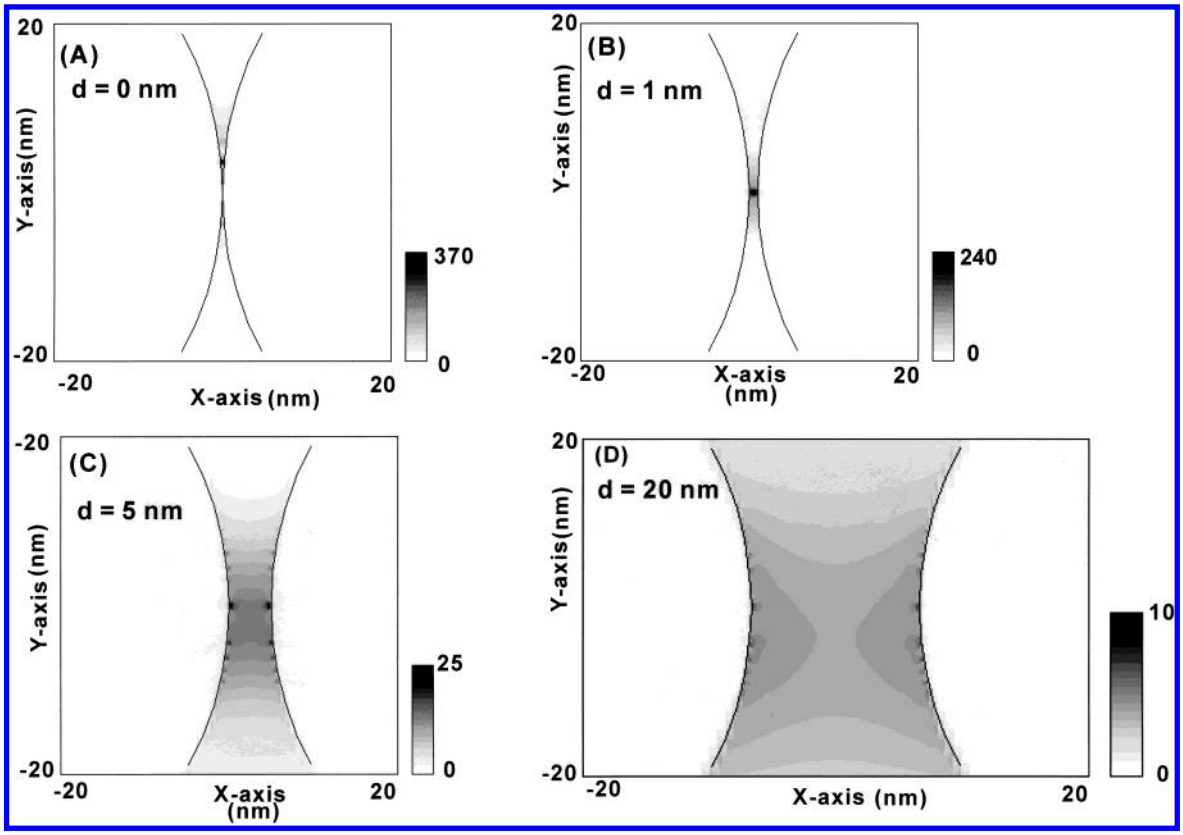


**Figure 12.** Electric field distribution for two touching Ag circular tubes ($r = 40$ nm) as a function of the spacing at 480 nm (wavelength): (a) $d = 0$ nm, (b) $d = 1$ nm, (c) $d = 5$ nm, and (d) $d = 20$ nm.

electronic resonance as in dye molecules, may critically contribute to give detectable signal from single molecule, as the blinking of Raman signal from R6G or other dye molecules are much more feasibly observed compared to DNA base.[9,10] Further study with different adsorbates is necessary to get deeper insight into the physical background behind SMS−SERS mechanism and to establish it as an analytical tool.

**3.3. Origin of the Blinking.** As described in the Introduction, SERS activity depends on the detailed morphology, size, and aggregation state. Then, we combined a Raman microscope with AFM to observe the scattered light image, Raman image as well as Raman spectra for individual Ag particles, whose morphology is characterized. This is crucial to explore the optimum condition for Ag particles to utilize the LSP most efficiently.[9,10] Actually, it enables us to identify each Ag particle in the optical, Raman, and AFM images. Consequently, the observed Ag particles with vast enhancement are aggregates with a size less than ca. 1 $\mu$m, which show stronger signals for polarization parallel to the connection axis. These particles show the blinking that the Raman intensity from R6G dye or DNA base adenine drastically and repeatedly changes as a function of time. In addition, the fluctuation of the peak frequency with ca. 10 $cm^{-1}$ and narrower bandwidth than that for higher surface coverage (ca. 1/2) were observed.[10] From these observations, possibilities such as fast orientation change of adsorbed molecule like a libration, relaxation via triplet electronic state, or photochemical bleaching are neglected.[10] The origin of the blinking is most probably due to thermal diffusion of an individual molecule on the Ag particle. It can be rationalized if (1) the Ag surface would have different sites with distinct enhancement and (2) there is sufficiently large thermal energy to overcome an activation barrier for the diffusion.

Other possibilities, such as geometrical morphology changes with heating by a pulse laser illumination with a power density

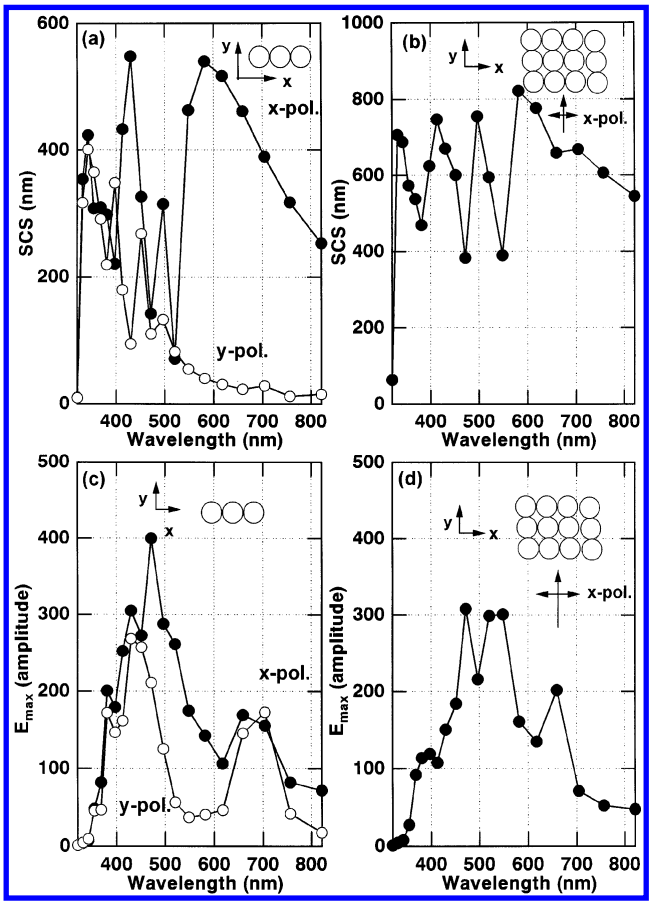


**Figure 13.** Scattering cross section (a, b) and local field distribution (c, d) for ordered multiparticles: (a, c) three particles in a line; (b, d) $3 \times 4$ matrix particles.

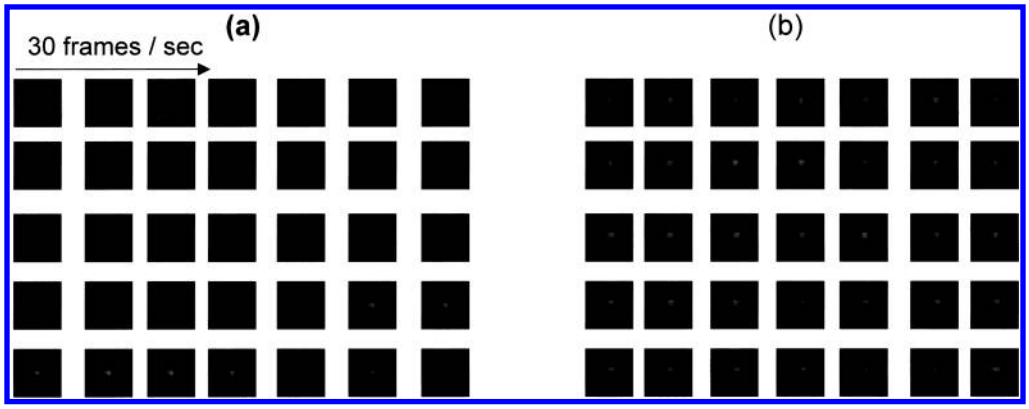


**Figure 14.** Observed temperature dependence of the blinking in SERS image for the same particles (see text for details): (a) at room temperature and (b) at 77 K. The blinking is suppressed at 77 K as the bright spot shows invariant intensity, in contrast to the intermittent SERS signal at room temperature.

of several millijoules per square centimeter in 5 ns,[34] are also ignored in our case. In that case, $10^5$ times larger number of photons are given to raise the sample temperature by up to about half the melting point for bulk Ag, and thus they observed significant difference in the PSTM (photon scanning tunneling microscope) image from semicontinuous Ag films after irradiation. In contrast, we used 40 W/cm$^2$ for Raman image capture, corresponding 40 nJ/ns, and confirmed by AFM measurement that our Ag particles do not change their morphology by laser illumination even with 1 order of magnitude higher laser power. Weiss and Haran[36] reported for R6G on Ag particles using 532 nm excitation that (1) background intensity as well as SERS signal shows the intensity fluctuation, (2) fluctuation rate is proportional to laser power, and (3) thermal effect is negligible as the sample temperature does not increase at all. Then, they concluded the origin of the blinking is possibly due to molecular desorption triggered by electron tunneling between the metal surface and molecules. In contrast, Michaels et al.[8] reported that there is no apparent correlation between the laser intensity and the frequency of fluctuations for R6G on Ag aggregates, using an $Ar^+$ laser at 514.5 nm. Although we cannot ignore their results, however, at least in our case pronounced background intensity was not observed, and moreover, relative intensity of different Raman bands from R6G does not significantly change during the blinking[10] with the excitation wavelength of 488 nm. Further study is necessary to confirm these discrepancies and reach definite conclusions.

In this paper, it was demonstrated that the vast enhancement of $10^{10}-10^{11}$ at SMS level[29] with the LSP resonance was obtained at the junction of two touching particles with various shapes and sizes as well as the sharp edge of triangular nanostructures. In particular, the parallel polarization gives much larger values by a factor of 100−1000 than that for perpendicular polarization, in good agreement with the observations.[9,10] The SMS by the LSP excitation agrees with the experimental results that DNA base shows the blinking as well as dye molecules. In this case a DNA base such as an adenine molecule has no electronic transition at a visible wavelength that possibly causes the charge-transfer resonance or additional enhancement by electronic resonance. It is plausible for molecules to diffuse on the Ag surface with a particular distance and activation energy,[30] although we have only little information on activation energy for adsorbed molecules on metal surfaces in ambient condition.[35] In addition, the blinking itself should be suppressed or the blinking frequency should be diminished at low temperature compared to room temperature if it results from thermal diffusion. Actually, we observed the blinking of SERS signal from R6G on Ag particles is suppressed at 77 K in the Raman image of Figure 14. In this experiment, the sample with surface coverage of ca. 1 molecule/Ag particle was immobilized on to the glass substrate and observed under the microscope.[10] At first, the blinking particles in the Raman image were found at room temperature (see Figure 14a). The sample was then cooled to 77 K with a liquid-nitrogen cryostat from Oxford, while the sample position in the Raman image was maintained by a precisely adjustable $X-Y$ stage. Thus we observed the Raman image for the same particles at 77 K as at room temperature. In fact this type of experiment is possible in our case, since we have a gridlike marker on the glass substrate with a space of 30 $\mu$m × 30 $\mu$m and only a countable number of particles were dispersed in each section. As clearly depicted in Figure 14b, the intensity from the blinking particles at room temperature does not change at 77 K with duration of time. Similar results were obtained for different aggregates, although detailed features of blinking at low temperature are further being studied. From these experiments, it was suggested that the blinking is raised from a thermal diffusion of molecule between the particular sites with vast enhancement and modest enhancement on Ag surfaces. These are most probably attributed to the junction of touching particles and other ordinary sites far from the junctions, respectively.

## 4. Summary

To explain the SMS−SERS in the framework of the LSP excitation, we have evaluated the local electric field on Ag particles with various shapes and sizes in nanoscale. The vast enhancement that corresponds to single-molecule sensitivity was obtained at the junctions of two touching Ag particles with different shapes, e.g., circular, ellipsoidal, triangular, or tetrahedral nanowires, and with different sizes, e.g., spheres with radii between 20 and 160 nm. Similar enhancement was obtained at the edge of isolated triangular particles. This is attributed to the confinement of the electric field in addition to coupling of the LSP at each particle, which possesses polarization dependence and decays within ca. 1 nm irrespective of particle size and morphology. The blinking probably arises from thermal diffusion between the junction with vast enhancement and other ordinary sites with modest enhancement. This is supported by aforementioned theoretical simulation and actually evidenced by suppression of the blinking at 77 K. The next step for us is to evaluate the scattering cross section and local electric field for metal particles with more complicated structures using the three-dimensional FDTD method in addition to participating dielectric properties of adsorbates in the local field evaluation. In addition, it is crucial to observe the hot sites and spatial

distribution of the near-zone field over the metal nanoparticles with SNOM and near-field Raman spectroscopy.

**Acknowledgment.** This work was supported by the Core Research for Evolutional Science and Technology (CREST) project of Japan Science and Technology Corporation (JST), by Grant-in-Aid for Scientific Research (B) 14340189 by Japan Society for the Promotion of Science (JSPS), and also by New Energy Development Organization (NEDO).

## References and Notes

(1) Otto, A.; Mrozek, I.; Grabhorn, H.; Akemann, W. *J. Phys.: Condens. Matter* **1992**, *4*, 1143.

(2) Kerker, M. *Surface Enhanced Raman Scattering*; SPIE, The International Society for Optical Engineering: Bellingham, WA, 1990; Vol. MS10.

(3) Krug, J. T.; Wang, G. D.; Emory, S. R.; Nie, S. *J. Am. Chem. Soc.* **1999**, *121*, 9208.

(4) Nie, S.; Emory, S. R. *Science* **1997**, *275*, 1102.

(5) Kneipp, K.; Kneipp, H.; Itzkan, I.; Dasari, R. R.; Feld, M. S. *Chem. Rev.* **1999**, *99*, 2957.

(6) Xu, H.; Aizpurua, J.; Käll, M.; Apell, P. *Phys. Rev.* **2000**, *E62*, 4317.

(7) Michaels, M.; Nirmal, M.; Brus, L. E. *J. Am. Chem. Soc.* **1999**, *121*, 9932.

(8) Michaels, M.; Nirmal, M.; Brus, L. E. *J. Phys. Chem.* **2000**, *B104*, 11965.

(9) Futamata, M.; Maruyama, Y.; Ishikawa, M. *Vib. Spectrosc.* **2002**, *30*, 17.

(10) Maruyama, Y.; Ishikawa, M.; Futamata, M. *Chem. Lett.* **2001**, 834.

(11) Rigler, R., Orrit, M., Basche, T., Eds. *Single Molecule Spectroscopy*; Springer Series in Chemical Physics; Springer: Berlin, 2002; Vol. 67, Chapt. 9 and 10.

(12) Kudelski, A.; Pettinger, B. *Chem. Phys. Lett.* **2000**, *321*, 356.

(13) Jensen, T. R.; Schatz, G. C.; Van Duyne, R. P. *J. Phys. Chem.* **1999**, *B103*, 2394.

(14) Aravind, P. K.; Metiu, H. *Surf. Sci.* **1983**, *124*, 506.

(15) Liver, N.; Nitzan, A.; Gersten, J. I. *Chem. Phys. Lett.* **1984**, *111*, 449.

(16) **)** Futamata, M.; Bruckbauer, A. *Chem. Phys. Lett.* **2001**, *341*, 425.

(17) Futamata, M.; Bruckbaur, A. *Jpn. J. Appl. Phys.* **2001**, *40*, 4423.

(18) Kolb, D. M.; Ullmann, R.; Ziegler, J. C. *Electrochim. Acta* **1998**, *43*, 2751.

(19) Kottmann, J. P.; Martin, O. J. F.; Smith, D. R.; Schultz, S. *Chem. Phys. Lett.* **2001**, *341*, 1.

(20) Kottmann, J. P.; Martin, O. J. F.; Smith, D. R.; Schultz, S. *Phys. Rev.* **2001**, *B64*, 1.

(21) Haynes, C. L.; Van Duyne, R. P. *J. Phys. Chem.* **2001**, *B105*, 5599.

(22) Yee, K. S. *IEEE Trans. Antennas Propag.* **1966**, *14*, 302.

(23) Chew, H.; Kerker, M. *J. Opt. Soc. Am.* **1985**, *B2*, 1025.

(24) Taflove, A., Ed. *Computational Electrodynamics: the finite-difference time-domain method* (2nd ed.); Artech House: Norwood, MA, 2000.

(25) Hildebrandt, P.; Stockburger, M. *J. Phys. Chem.* **1984**, *88*, 5935.

(26) Bohren, C. F.; Hoffman, D. R. *Adsorption and Scattering of Light by Small Particles*; John Wiley & Sons: New York, 1983; p 344.

(27) Wada, Y.; Tsukada, M.; Fujihira, M.; Matsushige, K.; Ogawa, T.; Haga, M.; Tanaka, S. *Jpn. J. Appl. Phys.* **2000**, *39*, 3835.

(28) Otto, A. *Phys. Stat. Solid* (a) **2001**, *188*, 1455.

(29) The factor of $10^{14}$ is referred as the value for SMS based on the comparison with fluorescence spectroscopy. In our facility, however, the enhancement necessary for SMS is $10^{10}$ as explained here. Detected photons for Raman scattering from a single molecule is given by $N_{obs} = (N_L/S)\rho_S S \times \int (d^2\sigma/d\Omega\, d\omega)\, d\omega\, \Delta\Omega\eta_{sys}$. Here $N_{obs}$ = detected signal counts, $(N_L/S)$ = incident photon numbers per unit area, $\rho_S$ = molecular density (molecules/area), $S$ = irradiated area, $(d^2\sigma/d\Omega\, d\omega)$ = differential scattering cross section, and $\eta_{sys}$ = spectrometer efficiency × detector sensitivity/efficiency (counts/photon). When the incident $Ar^+$ laser power is 100 $\mu$W/$\mu$m$^2$ at 488 nm, the photon flux of $2.5 \times 10^{14}$ photons/s irradiates the sample. If the scattering cross section of the sample is enhanced to $10^{-16}$ cm$^2$, similar to the fluorescence signal, a Raman signal of 37 500 counts/s is obtained from the parameters $(N_L/S) = 100\ \mu W/\mu m^2 = 2.5 \times 10^{22}$ photons/(s·cm$^2$), $\rho_S S = 1$, $(d^2\sigma/d\Omega\, d\omega) = 10^{-16}$ cm$^2$, and $\eta_{sys} = Q_{poly}Q_e A = 0.3 \times 0.5 \times 0.1 =$ ca. 0.015. The signal intensity is much stronger than the detection limit as the noise level of our facility is ca. 1 count/s. Thus, the enhancement of $1.3 \times 10^{10}$ is sufficient to detect the Raman signal from an isolated molecule with a signal-to-noise ratio of 5 according to $10^{14}/(37\,500/5) = 1.3 \times 10^{10}$. As reported in this paper, this value can be achieved only with electromagnetic mechanism.

(30) The possibility for a molecule to jump to the next site is given by $f = Z\nu \exp(-Q_d/kT)$ in a one-dimensional diffusion model. Here $f$ = frequency to jump to the next site (in reciprocal seconds); $Z$ = number of nearest-neighbor sites, e.g., 4; $\nu$ = frequencies to try to move over the barrier (frequencies of molecular vibrations, in reciprocal seconds), $Q_d$ = adsorption energy (potential barrier), 40 kJ/mol = $6.6 \times 10^{-20}$ J/molecule for physisorption; and $kT$ = thermal energy, $(1.38 \times 10^{-23}\ J\ K^{-1}) \times T$ (in kelvins). For instance, $f = 4.1 \times 10^5\ s^{-1}$ at 300 K and $8.7 \times 10^{-17}\ s^{-1}$ at 77 K is estimated for physisorption, although the actual energy barrier for adsorbed molecule to diffuse to the nearest neighbor sites must be much smaller than 40 kJ/mol. Next we should consider the path length for molecules to reach the particular site with distinct enhancement from ordinary sites with modest enhancement. According to our calculation, the maximum field is concentrated only at the junction within ca. 5 nm at most (see Figures 12A and 6C,D). If we accumulate the average effective length for ca. 0.3 s (blinking frequency) based on the above equation, the distance 5 nm is a possible value for molecules to diffuse. Thus, the blinking can be suppressed or the frequency is diminished at low temperature by losing the thermal energy.

(31) As the first-order approximation, the vast amplitude enhancement of >330 for the incident field was obtained at the junction yields to the Raman scattering enhancement of $>10^{10}$, because the scattering intensity from induced Raman dipole is resonantly enhanced by the LSP excitation of metal particles as well as incident channel, and thus is approximately proportional to fourth power of incident electric field as $I_{Raman} \propto |E_s \alpha E_i|^2 \approx |E_i|^4 \alpha^2$ (here $E_s$, $\alpha$, and $E_i$ are scattering field, Raman tensor, and incident field intensity, respectively). The value $10^{10}$ corresponds to the single-molecule sensitivity as it yields a detectable signal of 5−10 counts/s with our facility.[9,10]

(32) Stäckle, R. M.; Suh, Y. D.; Deckart, V.; Zenobi, R. *Chem. Phys. Lett.* **2000**, *318*, 131.

(33) Hayazawa, Y.; Inoue, Y.; Sekkat, Z.; Kawata, S. *Chem. Phys. Lett.* **2001**, *335*, 369.

(34) Ducourtieux, D.; Podolskiy, V. A.; Grésillon, S.; Buil, S.; Berini, B.; Gadenne, P.; Boccara, A. C.; Rivoal, J. C.; Bragg, W. D.; Bareijee, K.; Safonov, V. P.; Drachev, V. P.; Ying, Z. C.; Sarychev, A. K.; Shalaev, V. M. *Phys. Rev.* **2001**, *B64*, 165403.

(35) Barth, J. V. *Surf. Sci. Rep.* **2000**, *40*, 75.

(36) Weiss, A.; Haran, G. *J. Phys. Chem.* **2001**, *B105*, 12348.

(37) Wang, D. S.; Kerker, M. *Phys. Rev.* **1981**, *B24*, 1777.